

# Electrospinning synthesis of 3D porous NiO nanorods as anode material for lithium-ion batteries

XIANG WEI KONG<sup>1</sup>, RONG LIANG ZHANG<sup>1,\*</sup>, SHENG KUI ZHONG<sup>2</sup>, LING WU<sup>2</sup>

<sup>1</sup>School of Metallurgical and Materials Engineering, Jiangsu University of Science and Technology, Zhangjiagang 215600, China

<sup>2</sup>School of Iron and Steel, Soochow University, Suzhou 215021, China

Three-dimensional NiO nanorods were synthesized as anode material by electrospinning method. X-ray diffraction results revealed that the product sintered at 400 °C had impure metallic nickel phase which, however, became pure NiO phase as the sintering temperature rose. Nevertheless, the nanorods sintered at 400, 500 and 600 °C had similar diameters (~200 nm). The NiO nanorod material sintered at 500 °C was chip-shaped with a diameter of 200 nm and it exhibited a porous 3D structure. The nanorod sintered at 500 °C had the optimal electrochemical performance. Its discharge specific capacity was 1127 mAh·g<sup>-1</sup> initially and remained as high as 400 mAh·g<sup>-1</sup> at a current density of 55 mA·g<sup>-1</sup> after 50 cycles.

Keywords: *Li-ion battery; anode; charging/discharging; NiO; nanorod*

© Wrocław University of Technology.

## 1. Introduction

Lithium-ion batteries have recently been widely applied as an important energy source of new energy vehicles. However, commercialized lithium-ion battery anode materials [1, 2], which are mostly made of carbon materials, have some disadvantages. For example, metallic lithium and carbon have similar electric potentials, which causes precipitation of lithium dendrites resulting in short circuit. In comparison, NiO discharge platform is generally higher than that of graphite [3–5], which can avoid lithium dendrites to some extent and improve the safety performance of the batteries. Since the theoretical specific capacity of NiO (718 mAh·g<sup>-1</sup>) evidently exceeds that of graphite, it is of great practical significance to develop a new generation of high-capacity lithium-ion batteries. Moreover, it has attracted global attention due to abundant reserve of that material and high cost-effectiveness.

However, the electrochemical performances of NiO materials vary significantly owing to the differences between particle size and morphology.

Micron-sized NiO has low irreversible capacity and can hardly be cycled. According to the conversion reaction mechanism, discharge of NiO is bound to generate a large amount of low-density lithium oxide, rendering electrode to rapidly expand. With accumulation of stress, capacity fading occurs because active substance finally falls off the collector. To solve this problem, the electrospinning method [6–11] has been employed to prepare nano-sized lithium-ion battery anode materials [12–17], by which NiO enjoys improvement of capacity retention.

In this study, 3D porous NiO nanorods were synthesized by combined sol-gel electrospinning method as anode materials for lithium-ion batteries, and their morphology, structure and electrochemical performance were determined.

## 2. Experimental

### 2.1. Preparation of NiO nanofibers by electrospinning

NiO precursor nanofibers were prepared by using a combined sol-gel electrospinning technique. Preparation of the precursor was

\*E-mail: zhangrljx19201@163.com

the most important step in the synthesis of the fibers. The precursor solution for electrospinning was made from polyvinylpyrrolidone (Aladdin), ethanol,  $\text{Ni}(\text{CH}_2\text{COO})_2 \cdot 4\text{H}_2\text{O}$  and acetic acid. Firstly, an ethanol solution containing 8 wt.% polyvinylpyrrolidone was prepared under vigorous stirring for more than 12 h to get a transparent liquid (18 g). Then nickel acetate (7.5 g) was added into acetic acid (15 g) that was continuously stirred at 50 °C for 4 h to get a green homogeneous solution. Finally, the solution was dropwise added into the prepared transparent liquid, giving a green homogeneous solution after magnetic stirring. The precursor sol was placed in a plastic syringe and delivered to a conducting spinneret that fed the sol at a rate of  $0.5 \text{ mL} \cdot \text{h}^{-1}$ . A high voltage power supply was used to provide a 12 kV voltage for the as-prepared electrospinning solution. A piece of flat aluminum foil was used to collect the nanofibers. The distance between the tip of the dropper and the collector was 15 cm. In the electric field, a polymer jet was ejected and accelerated toward the counter electrode. The solvent evaporated rapidly as the high-surface-area steam traveled to the target. Dry fibers accumulated randomly on the collection screen and were collected as a fibrous mat. The PVP-NiO composite nanofibers were then heated at a rate of  $2 \text{ }^\circ\text{C} \cdot \text{min}^{-1}$  up to 400 °C, 500 °C and 600 °C, respectively, and then sintered for 5 h in air to obtain the pure NiO nanorods.

## 2.2. Characterization

Powder X-ray diffractometer (XRD, Rint-2000, Rigaku) using  $\text{CuK}\alpha$  radiation was employed to identify the crystalline phase of the samples. XRD Rietveld refinement was performed by MAUD (Material Analysis Using Diffraction) method. Morphology of the powders was observed by scanning electron microscope (SEM, JEOL, JSM-5600LV).

## 2.3. Electrochemical tests

Electrochemical performance was tested using a CR2025 coin-type cell of  $\text{Li}/\text{LiPF}_6$  (EC: DMC = 1:1 in volume)/NiO. The working

cathode was composed of 80 wt.% active material, 10 wt.% acetylene black as a conducting agent and 10 wt.% poly(vinylidene fluoride) as a binder. After being blended in N-methyl pyrrolidinone, the mixed slurry was spread uniformly on a copper foil and dried in vacuum for 12 h at 120 °C. A metallic copper foil was used as an anode. Electrodes were punched in the form of 14 mm diameter disks, and the typical positive electrode loadings were in the range of  $4.0 \text{ mg} \cdot \text{cm}^{-2}$  to  $4.5 \text{ mg} \cdot \text{cm}^{-2}$ . A microporous polypropylene film was used as the separator. The cells were assembled in a dry argon-filled glove box, and then charged and discharged over a potential range of 0.01 V to 3 V versus  $\text{Li}/\text{Li}^+$  electrode at 25 °C. Cyclic voltammetry (CV) tests were carried out with a CHI660D electrochemical analyzer, and CV plots for the cells were recorded in the potential range of 0.01 V to 3 V.

## 3. Results and discussion

### 3.1. XRD pattern analyses

Fig. 1 shows the XRD patterns of materials calcined at various temperatures. All three lines show diffraction peaks at  $37.3^\circ$ ,  $43.3^\circ$ ,  $62.9^\circ$ ,  $75.4^\circ$  and  $79.4^\circ$ , corresponding to the (1 1 1), (2 0 0), (2 2 0), (3 1 1) and (2 2 2) crystal planes of cubic NiO, respectively. The sample prepared at 400 °C still contained Ni metal. At 500 °C and 600 °C, however, pure NiO phase was obtained.

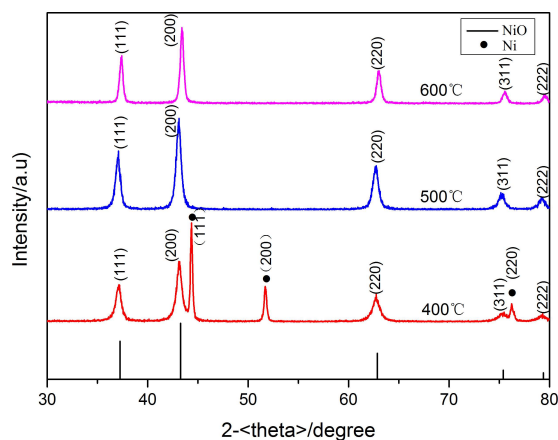


Fig. 1. XRD patterns of NiO nanofibers sintered at different temperatures.

As the calcination temperature increases, the widths of diffraction peaks gradually decrease, suggesting that NiO prepared at a higher sintering temperature crystallized better. In order to study the grain size of NiO nanorod prepared by the electrospinning method, the Scherrer equation ( $D = K\lambda/(\beta\cos\theta)$ ) was used, where  $D$  represents the grain size;  $K$  is a constant related to the crystal (0.89);  $B$  is the half-height width of diffraction peak;  $2\theta$  is the corresponding diffraction angle;  $K$  is the X-ray wavelength (0.15418 nm). The NiO nanorod grain sizes at 400 °C, 500 °C and 600 °C, were estimated by using  $D$  as 14.9 nm, 16.2 nm and 22.1 nm, respectively. Clearly, NiO nanorod grains gradually grew as the sintering temperature increased.

### 3.2. Morphology and microstructure

Fig. 2 shows the SEM images of the precursor nanofibers. The precursor nanofibers have smooth surfaces with the precursor ( $\text{Ni}(\text{Ac})_2/\text{PVP}$  composite) randomly oriented in the continuous internal structure. The average diameter of as-spun fibers is about 300 nm.

Fig. 3a to Fig. 3f show the SEM images of NiO nanofibers sintered at different temperatures. After being sintered at different temperatures, the 3D structure remains without significant structural deformation. However, both diameter and length of the NiO nanorods decrease to 200 nm after sintering, which can be ascribed to removal of the PVP matrix and crystallization of NiO. Furthermore, the NiO nanorods become porous-surfaced and shorten to about 1.5  $\mu\text{m}$  after sintering. Nevertheless, the nanorods sintered at 400 °C, 500 °C and 600 °C have similar diameters ( $\sim 200$  nm). EDS mappings of the sample calcined at 500 °C show that Ni and O are distributed uniformly in the NiO nanorods (Fig. 3g and Fig. 3h).

### 3.3. Electrochemical tests

Fig. 4 shows the charge-discharge curves of the NiO nanorods in the first and second cycles in the potential range of 0.01 V to 3.0 V. The sample delivers initial discharge capacities of 773  $\text{mAh}\cdot\text{g}^{-1}$  (400 °C), 1127  $\text{mAh}\cdot\text{g}^{-1}$  (500 °C)

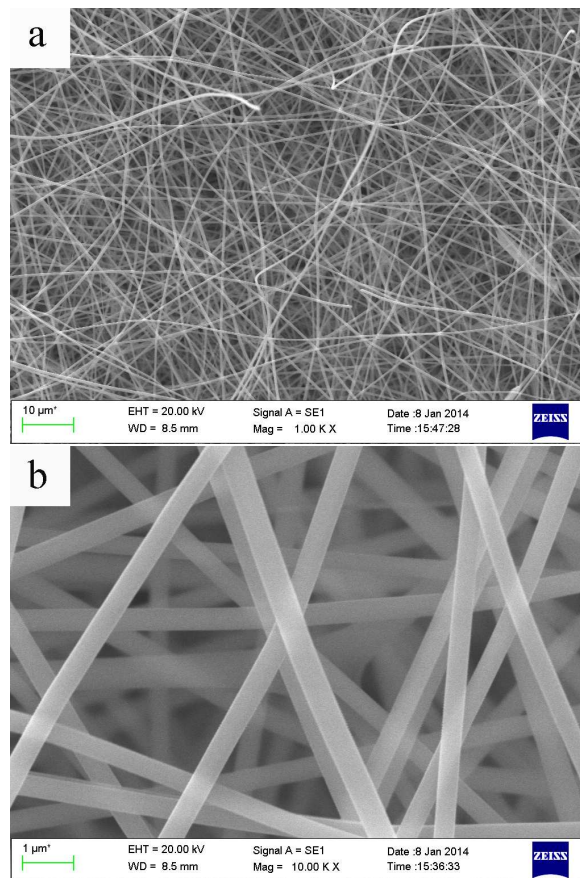


Fig. 2. SEM images of precursor nanofibers.

and 1256  $\text{mAh}\cdot\text{g}^{-1}$  (600 °C), which all exceed the theoretical one (718  $\text{mAh}\cdot\text{g}^{-1}$ ), indicating good cyclic reversibility. NiO was reduced by Li in the discharge process, so the original NiO structure was disrupted, forming nano-sized metal Ni and amorphous  $\text{Li}_2\text{O}$ . During charging, the Ni metal nanoparticles reacted with  $\text{Li}_2\text{O}$  and generated NiO and Li. Accordingly, the discharge capacity mainly originated from the reversible redox reaction ( $\text{NiO} + 2\text{Li} \leftrightarrow \text{Ni} + \text{Li}_2\text{O}$ ). However, in the discharge process, as the catalytic metal particles near the electrode decomposed the electrolyte, a solid electrolyte film (SEI) formed [16, 17] and during the first few cycles, the film thickened until stabilization. The SEI film decreased electron conductivity by increasing polarization resistance. As a result, the capacity was severely attenuated in the initial charge-discharge process, accompanied by the higher-than-theoretical capacity and the larger irreversible capacity of initial discharge.

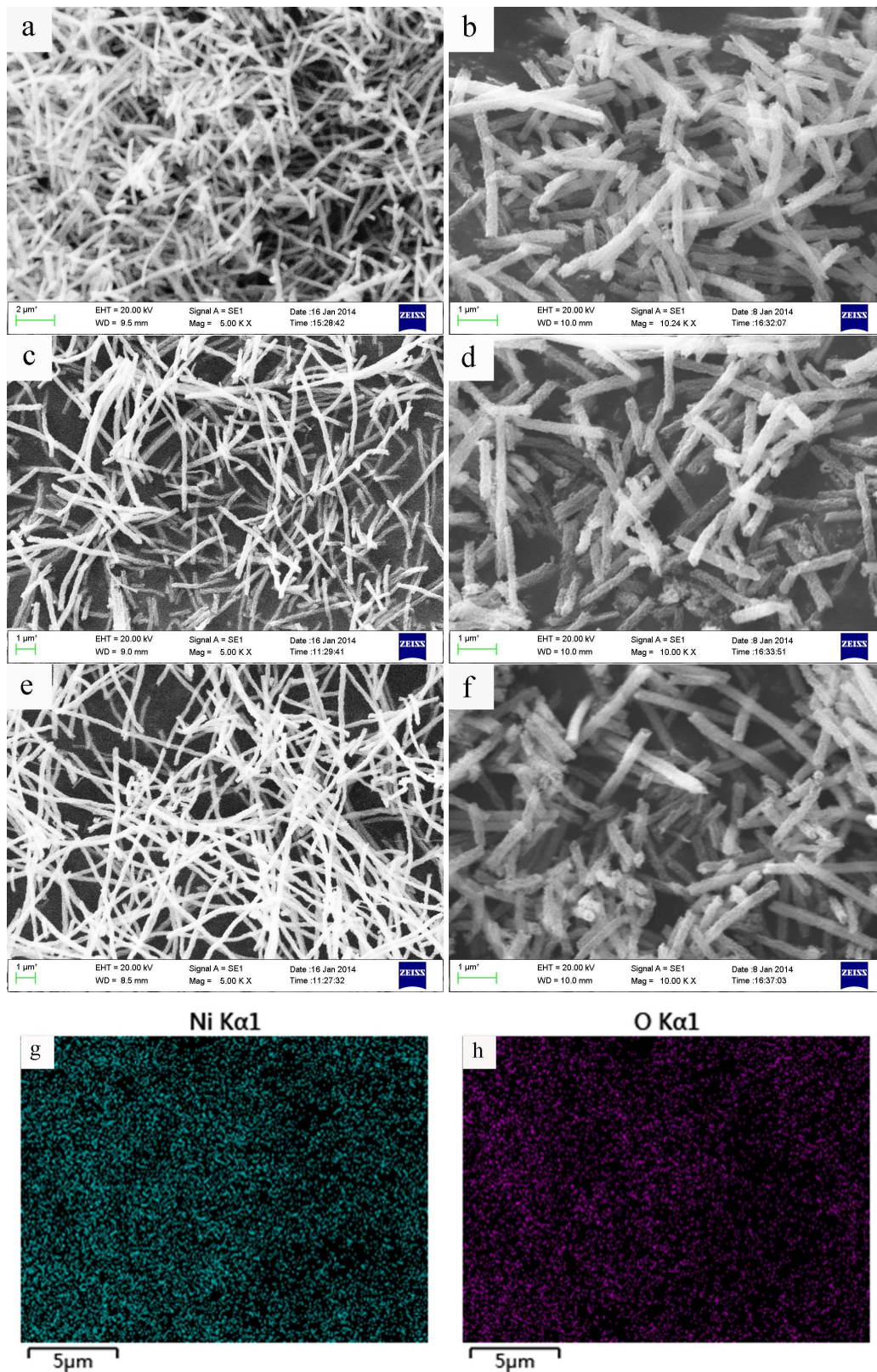


Fig. 3. SEM images of NiO nanofibers sintered at different temperatures: 400 °C (a, b), 500 °C (c, d) and 600 °C (e, f). EDS mappings of Ni (g) and O (h) of the sample calcined at 500 °C.

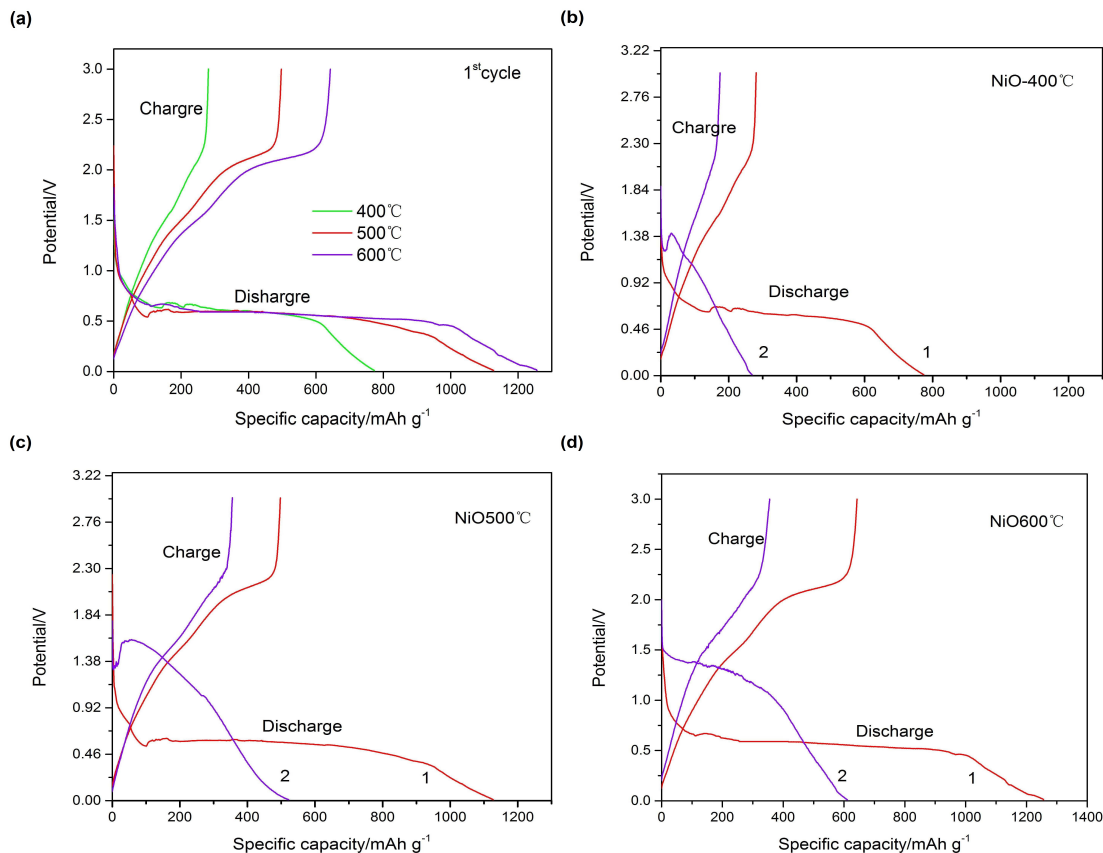


Fig. 4. Charge-discharge curves of samples at different temperatures (current density:  $50 \text{ mA} \cdot \text{g}^{-1}$ ).

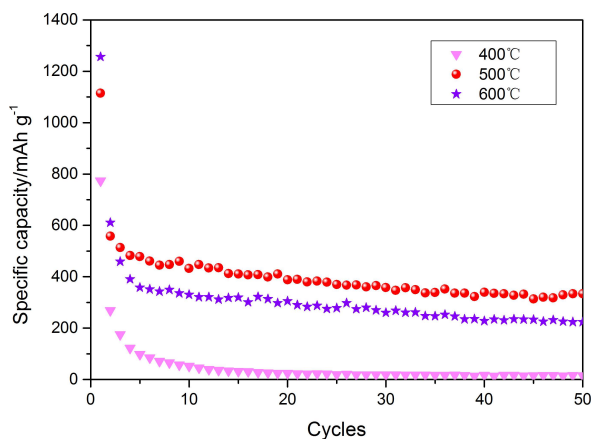


Fig. 5. Cycling performance of samples at different temperatures.

As presented in Fig. 5, the NiO nanorod sample prepared at  $600^\circ\text{C}$  shows the highest initial capacity ( $1256 \text{ mAh} \cdot \text{g}^{-1}$ ), but that synthesized at  $500^\circ\text{C}$  exhibits the best cycling performance. Hence, the

nano-NiO functioned less efficiently in the first charge-discharge cycle, but the charging and discharging efficiency gradually rose with increasing cycle.

Fig. 6 shows the C-V curves of the samples calcined at  $500^\circ\text{C}$ . As suggested by the distinct differences between the first and second cycles, the reversible specific capacity of the first cycle lost seriously, mainly because a layer of partially reversible SEI was generated on the electrode surface in the first discharge. That consumed part of Li and caused the decrease of specific capacity. The results accord well with those in Fig. 4a to Fig. 4c.

## 4. Conclusions

By using a combined sol-gel electrospinning method, we successfully synthesized chip-shaped NiO nanorods. XRD patterns showed that the product sintered at  $400^\circ\text{C}$  had impure metallic nickel

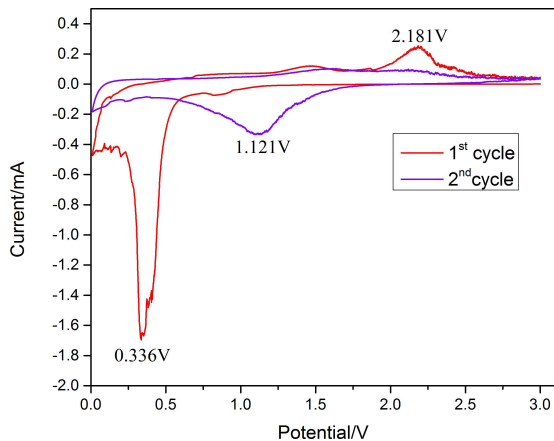


Fig. 6. C-V curves of samples calcined at 500 °C (scan rate: 0.05 mV·s<sup>-1</sup>).

phase which, however, became pure NiO phase as the sintering temperature rose. Nevertheless, the nanorods sintered at 400 °C, 500 °C and 600 °C had similar diameters (~200 nm). The NiO nanorods synthesized at 600 °C showed the highest initial capacity (1256 mAh·g<sup>-1</sup>), but those prepared at 500 °C had the best cycling performance. Although the nano-NiO was less efficient in the first charge-discharge cycle, the charging and discharging efficiency was gradually augmented as the cycle increased. After 50 cycles, the chip-shaped porous 3D NiO nanorods still had 99 % capacity retention at 400 mAh·g<sup>-1</sup>.

### Acknowledgements

This study was supported by the National Natural Science Foundation of China (51204114), the Natural Science Foundation of Jiangsu Province of China (BK2012216), the China Postdoctoral Science Foundation (2013M540464) and the University Graduate Student Scientific Research Innovation Projects of Jiangsu Province of China (CXLX14\_1083).

### References

- [1] ENDO M., KIM C., NISHIMURA K., FUJINO T., MIYASHITA K., *Carbon*, 38 (2000), 183.
- [2] AVELLANEDA D., NAIR M.T.S., NAIR P.K., *Thin Solid Films*, 517 (2009), 2500.
- [3] HEE P.S., HYOUNG K.C., *Rare Metals*, 25 (2006), 184.
- [4] MA J.M., YANG J.Q., JIAO L.F., MAO Y.H., WANG T.H., DUAN X.C., LIAN J.B., ZHENG W.J., *CrystEngComm*, 14 (2012), 453.
- [5] NAM I., KIM N.D., KIM G.P., PARK J., YI J., *J. Power Sources*, 244 (2013), 56.
- [6] LU C.D., GANGYI X., KAWAS J.R., *Small Ruminant Res.*, 89 (2010), 102.
- [7] DING B., KIMURA E., SATO T., FUJITA S., SHIRATORI S., *Polymer*, 45 (2004), 1895.
- [8] TANG K., YU Y., MU X.K., PETER A., AKEN V., MAIER J., *Electrochem. Commun.*, 28 (2013), 54.
- [9] WANG L., YU Y., CHEN P.C., ZHANG D.W., CHEN C.H., *J. Power Sources*, 183 (2008), 717.
- [10] FAN Q., WHITTINGHAM M.S., *Electrochem. Solid. St.*, 10 (2007), 48.
- [11] JI L.W., LIN Z., ZHOU R., SHI Q., TOPRAKCI O., MEDFORD A.J., *Electrochim. Acta*, 55 (2010), 1605.
- [12] CUI Q.Z., DONG X.T., WANG J.X., LI M., *J. Rare Earth*, 26 (2008), 664.
- [13] ZHANG X., THAVASI V., MHAISALKAR S.G., RAMAKRISHNA S., *Nanoscale*, 4 (2012), 1707.
- [14] DING Y.H., ZHANG P., LONG Z.L., JIANG Y., XU F., *J. Alloy. Compd.*, 487 (2009), 507.
- [15] FAN X., ZOU L., ZHENG Y.P., KANG F.Y., SHEN W.C., *Electrochem. Solid. St.*, 12 (2009), 199.
- [16] ARAVINDAN V., PALANISWAMY S.K., JAYARAMAN S., WONG C.L., SEERAM R., SRINIVASAN M., *J. Power Sources*, 227 (2013), 284.
- [17] SHIN J.Y., SAMUELIS D., MAIER J., *Adv. Funct. Mater.*, 21 (2011), 3464.

Received 2015-01-27

Accepted 2016-01-26